The Astronomical Journal, 129:1396–1411, 2005 March

THE OPACITY OF SPIRAL GALAXY DISKS. IV. RADIAL EXTINCTION PROFILES FROM COUNTS OF DISTANT GALAXIES SEEN THROUGH FOREGROUND DISKS

B. W. Holwerda,[1,2] R. A. Gonzalez,[3] Ronald J. Allen,[1] and P. C. van der Kruit[2]
Received 2004 September 22; accepted 2004 November 22

ABSTRACT

Dust extinction can be determined from the number of distant field galaxies seen through a spiral disk. To calibrate this number for the crowding and confusion introduced by the foreground image, González et al. and Holwerda et al. developed the Synthetic Field Method (SFM), which analyzes synthetic fields constructed by adding various deep exposures of unobstructed background fields to the candidate foreground galaxy field. The advantage of the SFM is that it gives the average opacity for the area of a galaxy disk without making assumptions about either the distribution of absorbers or of the disk starlight. However, it is limited by poor statistics on the surviving field galaxies, hence the need to combine a larger sample of fields. This paper presents the first results for a sample of 32 deep *Hubble Space Telescope* (*HST*)/WFPC2 archival fields of 29 spiral galaxies. The radial profiles of average dust extinction in spiral galaxies based on calibrated counts of distant field galaxies is presented here, both for individual galaxies and for composites from our sample. The effects of inclination, spiral arms, and Hubble type on the radial extinction profile are discussed. The dust opacity of the disk apparently arises from two distinct components: an optically thicker ($A_I = 0.5$–4 mag) but radially dependent component associated with the spiral arms and a relatively constant optically thinner disk ($A_I \approx 0.5$ mag). These results are in complete agreement with earlier work on occulted galaxies. The early-type spiral disks in our sample show less extinction than the later types. Low surface brightness galaxies, and possibly Sd's, appear effectively transparent. The average color of the field galaxies seen through foreground disks does not appear to change with radius or opacity. This gray behavior is most likely due to the patchy nature of opaque clouds. The average extinction of a radial annulus and its average surface brightness seem to correlate for the brighter regions. This leads to the conclusion that the brighter parts of the spiral disk, such as spiral arms, are also the ones with the most extinction associated with them.

Key words: astronomical data bases: miscellaneous — dust, extinction — galaxies: ISM — galaxies: photometry — galaxies: spiral — methods: statistical — radiative transfer — techniques: photometric

1. INTRODUCTION

The optical depth of spiral disks has been the topic of many and varied studies since the claim by Holmberg (1958) that they are transparent. The subject became controversial when Disney et al. (1989) and Valentijn (1990) argued that disks were virtually opaque. At the Cardiff meeting (Davies & Burstein 1995) many possible methods to attack the problem were proposed. The dust disks of spiral galaxies may obscure objects in the high-redshift universe (Alton et al. 2001; Ostriker & Heisler 1984) or conceal mass in their disks (Valentijn 1990; Cuillandre et al. 2001). An excellent review of the current state of knowledge on the opacity of spiral disks is given by Calzetti (2001).

Early approaches to this subject were presented in Davies & Burstein (1995), and more recent developments are as follows:

1. Disks are more opaque in the blue (Tully et al. 1998; Masters et al. 2003).
2. They are practically transparent in the near-infrared (Peletier & Willner 1992; Graham 2001), making these bands the best mass-to-luminosity estimator (de Jong 1996).
3. Disks are practically transparent in their outer parts but show significant absorption in the inner regions (Valentijn 1994; Giovanelli et al. 1994).
4. The extinction correlates with galaxy luminosity (Giovanelli et al. 1995; Tully et al. 1998; Masters et al. 2003).
5. Spiral arms are more opaque than the disk (Beckman et al. 1996; White et al. 2000).

The majority of these studies are based on either inclination effects on the light distribution of a large sample of disks or a dust and light model to fit the observed profiles.

While there is some agreement on the view that spiral disks are substantially optically thick in their central regions and become optically thin in their outer parts, the exact radial extinction profile remains uncertain. Most measurements to date use the disk light itself to measure the extinction and consequently require an assumption on the relative distribution of dust and light in a spiral disk.

The extinction in a disk can be derived from far-infrared and submillimeter emission arising from the cold dust in disks. However, these methods assume that the emission characterizes the dust in the disk. But the far-infrared and submillimeter emission is likely to be dominated by the warmest component of the dust, which tends to be the smaller grains on the outside of molecular clouds facing an energy source (Dale & Helou 2002; Helou et al. 2000). In this case the far-infrared and submillimeter emission underestimates the average opacity. Mayya & Rengarajan (1997) mention this problem in their estimate, based on *IRAS* observations, of the gas-to-dust ratio in spiral disks.

To obtain a better characterization of the absorption in a spiral disk without knowing the distribution of stars and dust in the disk, a known background source is needed. White & Keel (1992) proposed using an occulted galaxy for this purpose,

[1] Space Telescope Science Institute, 3700 San Martin Drive, Baltimore, MD 21218; holwerda@stsci.edu.
[2] Kapteyn Institute, Groningen Landleven 12, NL-9747 AD Groningen, Netherlands.
[3] Centro de Radioastronomía y Astrofísica, Universidad Nacional Autónoma de México, 58190 Morelia, Michoacán, Mexico.

TABLE 1
HST Archive Data Sample

Name	Exp. Time V_{F555W}	I_{F814W}	Prop. ID	Reference
NGC 925	26400.0	9000.0	5397	Silbermann et al. (1996)
NGC 1365	66560.0	16060.0	5972	Silbermann et al. (1999)
NGC 1425	58800.0	29700.0	5972/6431	Mould et al. (2000)
NGC 1637	26400.0	13200.0	9155	Leonard et al. (2002a, 2002b)
NGC 2541	28760.0	12760.0	5972	Ferrarese et al. (1998)
NGC 2841	26400.0	11000.0	8322	Macri et al. (2001)
NGC 3031 (M81)	2000.0	2000.0	9073	Liu et al. (2002)
NGC 3198	27760.0	12560.0	5972	Kelson et al. (1999)
NGC 3319	26400.0	10400.0	6431	Sakai et al. (1999)
NGC 3351 (M95)	31900.0	9830.0	5397	Graham et al. (1997)
NGC 3621-1	5200.0	7800.0	8584	Sakai et al. (2004)
NGC 3621-2	20759.0	7380.0	5397	Rawson et al. (1997)
NGC 3627 (M66)	58800.0	25000.0	6549	Saha et al. (1999)
NGC 4321 (M100)	32750.0	17150.0	5397	Ferrarese et al. (1996)
NGC 4414-1	1600.0	1600.0	8400	Hubble Heritage
NGC 4414-2	32430.0	10230.0	5397	Turner et al. (1998)
NGC 4496A	68000.0	16000.0	5427	Saha et al. (1996b)
NGC 4527	60000.0	25000.0	7504	Saha et al. (2001)
NGC 4535	48800.0	31200.0	5397/6431	Macri et al. (1999)
NGC 4536	68000.0	20000.0	5427	Saha et al. (1996a)
NGC 4548 (M98)	48500.0	30900.0	6431	Graham et al. (1999)
NGC 4559	2000.0	2000.0	9073	Cropper et al. (2004)
NGC 4571	10400.0	26400.0	6833	Macri et al. (1999), Pierce et al. (1994)
NGC 4603	58800.0	14800.0	6439	Newman et al. (1999)
NGC 4639	58800.0	13000.0	5981	Sandage et al. (1996)
NGC 4725	32430.0	10230.0	5397	Gibson et al. (1999)
NGC 6946	2000.0	2000.0	9073	Larsen (2004)
NGC 7331	40660.0	9860.0	5397	Hughes et al. (1998)
UGC 2302	15000.0	15600.0	8255	Bovill et al. (2003)
UGC 6614	10100.0	10100.0	8213	Kim & McGaugh (2002)
NGC 5194-1 (M51)	2000.0	2000.0	9073	Larsen (2004)
NGC 5194-2 (M51)	2000.0	2000.0	9073	Larsen (2004)

assuming that it has a symmetric light distribution (Domingue et al. 1999, 2000; White et al. 2000; Keel & White 2001a, 2001b). González et al. (1998) and the companion paper of this work (Holwerda et al. 2005) use the number of distant galaxies in the field as the background source, calibrating this number with simulations following their Synthetic Field Method (SFM). In Holwerda et al. (2005), we describe the details of this method.[4]

Both the occulting galaxy method and the SFM have the benefit of not using the disk's own light to measure the extinction. The drawbacks of the Keel & White method are the assumption of symmetry of both galaxies and the small number of suitable pairs available. The SFM is more universally applicable, but it is limited by the poor statistics. However, it does not need to make assumptions regarding the distribution of either the disk's light or the absorbers in it. The SFM does require high-resolution images from the *Hubble Space Telescope* (*HST*) and, because of crowding, remains limited to the arms and disk of spiral galaxies.

In this paper we report radial extinction profiles for spiral disks of different Hubble types based on 32 Wide Field Planetary Camera 2 WFPC2) fields in 29 galaxies of Hubble types Sab and later. In § 2 we describe the sample and its selection in detail. The SFM is briefly outlined in § 3; a more complete description of the method and the recent improvements we have made to it is given in the companion paper (Holwerda et al. 2005). In § 4 we discuss the radial profile of average opacity for individual galaxies, and in § 5 the composite average radial extinction profile for our entire sample. The effects of inclination, spiral arm prominence, and Hubble type on the profiles are discussed as well. Section 6 discusses the average $V - I$ color of the field galaxies we found, and § 7 the tentative relation between average surface brightness and opacity. We discuss some of the implications of our results and end with conclusions on disk opacity drawn on the basis of the numbers and colors of field galaxies seen through them.

2. THE *HST* ARCHIVE SAMPLE

Our sample of *HST*/WFPC2 fields was selected from the MAST archive at the Space Telescope Science Institute (STScI), based on criteria for both the target galaxy and the *HST* data. The total exposure times and original proposal identifications and references are listed in Table 1, and the basic data on the galaxies in Table 2. The total solid angle of this sample is 146 arcmin^2.

The foreground galaxy should be a spiral, ideally face-on, spanning enough sky to cover a significant number of field galaxies. This solid angle constraint limits the maximum distance for application of the SFM to approximately 30 Mpc. *HST* starts to resolve the disk population of spiral galaxies at close distances, making the field too crowded for field galaxy

[4] For the remainder of the paper *field galaxies* mean the distant background objects we count and *foreground galaxy* refers to the galaxy disk through which these distant galaxies are seen.

TABLE 2
BASIC DATA

Galaxy	Type	R.A. (deg)	Decl. (deg)	P.A. (deg)	Incl. (deg)	D_{25} (arcmin)	Distance[a] (Mpc)	Galactic Extinction (mag)	Remarks
NGC 925	SAbd	36.820469	33.578880	−70	62.48	11.22	9.16	0.147	
NGC 1365	SBb	53.401909	−36.140659	49	34.41	10.47	17.95	0.039	
NGC 1425	SBb	55.548061	−29.893511	−51	57.32	5.75	21.88	0.025	
NGC 1637	SAB(rs)c	70.367622	−2.858040	27	30.68	3.98	8.2	0.078	[b]
NGC 2541	SAcd	123.666969	49.061440	−7	56.63	6.31	11.22	0.097	
NGC 2841	SAb	140.511063	50.976479	−30	60.33	8.13	14.1	0.030	[c]
NGC 3031 (M81)	SA(s)ab	148.88826	69.06526	−38.5	58.87		3.63	0.155	
NGC 3198	SBc	154.979126	45.549690	37	61.77	8.51	13.80	0.024	
NGC 3319	SB(rs)cd	159.789719	41.686871	39	69.51	6.17	13.30	0.028	
NGC 3351 (M95)	SBb	160.990555	11.703610	−2	14.53	7.41	10.00	0.054	
NGC 3621	SAc	169.567917	−32.812599	−16	58.13	12.3	6.64	0.156	
NGC 3627 (M66)	SAB(s)b	170.062607	12.991290	1	57.38	9.12	10.05	0.063	
NGC 4321 (M100)	SABbc	185.728745	15.822380	−57	39.65	7.41	15.21	0.051	
NGC 4414	SAc	186.612869	31.223545	−20	48.70	3.63	17.70	0.038	
NGC 4496A	SBm	187.913361	3.939467	65	58.67	3.98	14.86	0.048	
NGC 4527	SAB(s)bc	188.535400	2.653810	67	70.73	6.17	14.1	0.043	[d]
NGC 4535	SABc	188.584625	8.197760	27	28.36	7.08	15.78	0.038	
NGC 4536	SAB(rs)bc	188.613037	2.187880	−70	62.61	7.08	14.93	0.035	
NGC 4548 (M98)	SBb	188.860123	14.496320	−60	22.48	5.37	16.22	0.074	
NGC 4559	SAB(rs)cd	188.990372	27.959761	−37	61.77	10.72	10.88	0.034	
NGC 4571	SA(r)d	189.234879	14.217357	75	23.07	3.63	14.9	0.091	[e]
NGC 4603	SA(rs)bc	190.229980	−40.976402	30	50.21	3.39	33.3	0.325	[f]
NGC 4639	SABbc	190.718140	13.257536	−25	43.95	2.75	21.98	0.050	
NGC 4725	SABab	192.610886	25.500759	47	45.25	10.72	12.36	0.023	
NGC 5194 (M51)	SA(s)bc	202.46957	47.19526	45.0	25.58	11.22	8.4	0.067	
NGC 6946	SAB(rs)cd	308.718048	60.153679	70	39.65	11.48	11.48	0.663	
NGC 7331	SAb	339.267090	34.415920	−12	57.38	10.47	14.72	0.176	
UGC 2302	SB(rs)m	42.285831	2.127265	60.0	1.0	4.79	14.7	0.156	[g]
UGC 6614	SA(r)a	174.811844	17.143578	−65	40.54	1.66	84.68	0.055	[h]

NOTE.—Units of right ascension are hours, minutes, and seconds, and units of declination are degrees, arcminutes, and arcseconds.
[a] All distances were taken from Freedman et al. (2001) with some exceptions, noted below.
[b] Leonard et al. (2002a, 2002b).
[c] Macri et al. (2001).
[d] Saha et al. (2001).
[e] Macri et al. (1999); Pierce et al. (1994).
[f] Newman et al. (1999).
[g] No distance from Cepheid method or supernovae available. Using NED data (1104 km s^{-1}) and $H_0 = 75$ km^{-1} Mpc^{-1}.
[h] No distance from Cepheid method or supernovae available. Using NED data (6351 km s^{-1}) and $H_0 = 75$ km^{-1} Mpc^{-1}.

identification (see González et al. 2003). This imposes a minimum distance of a few megaparsecs. The galaxies are type Sab and later, as plotted in Figure 1, according to de Vaucouleurs et al. (1991, hereafter RC3). No limit on inclination was imposed as long as spiral arms could be discerned.

The majority of this sample is from the Distance Scale Key Project. The project's observing strategy (Freedman et al. 1994, 2001) was geared toward maximizing the number of Cepheid variables detected. This resulted in the selection of fields in the optical disk of face-on later type spiral galaxies with a prominent arm visible. These selection criteria must be taken into account when interpreting the opacity measurements of these fields.

The sample of spiral disks has multiepoch imaging in the two photometric bands available, as the original science driver for many of these data sets was to sample the Cepheid light curves. The reacquisition resulted in a slight shift in the pointing at each epoch. The unintentional "dither" allowed us to drizzle the combined images to a pixel scale of 0.″05. The data reduction is described in detail by Holwerda et al. (2005). González et al. (2003) predicted that improved resolution would mainly benefit the statistics of distant galaxy counts in the Local Group. However, as the sample spans a range of distances and the statistics are likely to be poor, the maximum possible sampling was selected. The PC chip was not used for analysis because it often lies on the most crowded region, its noise characteristics are different from the WF chips, and there are fewer reference fields available for the SFM.

This sample of *HST* pointings was selected because it is reasonably uniform, which allows similar processing using Hubble Deep Field (HDF) background fields. The *HST*/WFPC2 pointing should neither be on the center of the galaxy, where crowding poses too great a problem, nor outside the disk of the target galaxy, where the expected opacity is likely too low to be measured with the SFM. We selected pointings with the F814W (I) and F555W (V) filters because the identification of objects is based on several parameters characterizing structure and on the $V - I$ color. A minimum exposure time of about 2000 s in both filters was adopted. The choice of filters and exposure time was on the basis of our earlier experiences with spiral and irregular galaxies (González et al. 1998; Holwerda et al. 2002) and to maximize the number of suitable fields.

3. SFM: CALIBRATING THE FIELD GALAXY NUMBERS

Holwerda et al. (2005) describe in detail the data reduction and the automated SFM, so we give only a short summary here. To calibrate the numbers of field galaxies found in the science

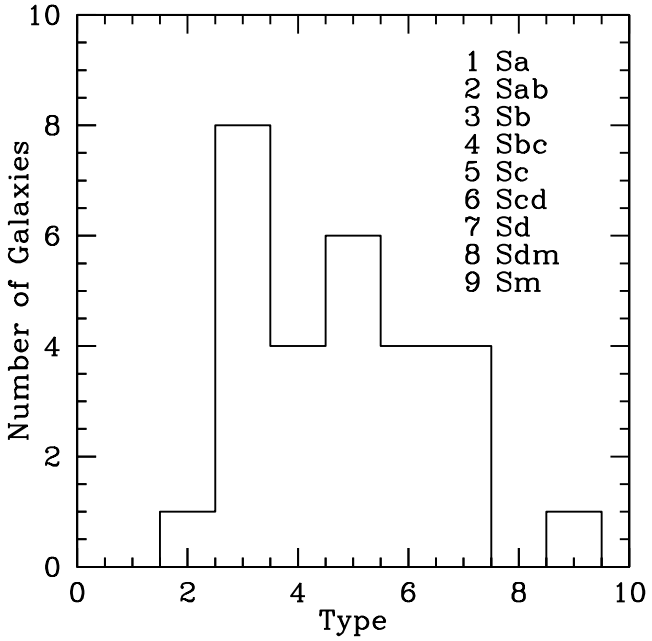

FIG. 1.—Distribution of Hubble type (de Vaucouleurs et al. 1991) for our *HST* sample. The Distance Scale Key Project (Freedman et al. 2001), from which most of our sample is drawn, concentrated on later types to maximize the number of Cepheids.

fields, simulated, or "synthetic," fields are made. These are the original science fields with an extincted HDF added. The numbers of simulated field galaxies found suffer from the same confusion and crowding as the number from the science field and therefore depend solely on the dimming applied. A series of simulations gives us the relation between field galaxy numbers and applied dimming. The following relation is fitted to the simulated numbers:

$$A = -2.5C \log(N/N_0), \quad (1)$$

where A is the dimming in magnitudes, N the number of field galaxies in a simulation, and N_0 and C are the normalization and slope of the fit, respectively (i.e., the number of field galaxies expected with no extinction and how this number diminishes with increasing extinction). The slope C characterizes the effects of crowding and confusion on the relation between opacity and galaxy numbers. It is usually slightly over unity, but the unique character of each field led us to characterize C using the simulations in each field or combination of fields. The intersection between this relation and the *real* number of field galaxies gives us the average extinction (A_I) typical for the solid angle where these field galaxies were found. The field galaxies are identified in the science fields using automated selection, based on structural parameters and $V - I$ color together with a visual verification. In the synthetic fields the visual check of objects was substituted by anticorrelating the automatically selected objects with the automatic selection in the science field, removing both the real distant galaxies and contaminants and leaving only added objects.

The uncertainty in the number of field galaxies from the science field is a combination of the Poisson uncertainty and the uncertainty due to field galaxy clustering. The uncertainty in the simulated numbers is Poisson only because they come from a known background, the HDFs. The uncertainty in average opacity is derived from the uncertainties in field galaxy numbers on the basis of the Poisson uncertainty as expressed by Gehrels (1986), and the clustering uncertainty based on the two-point correlation function found by Cabanac et al. (2000) and equation (1). The crowding and confusion bias is calibrated with the simulations. For a detailed error discussion of the SFM see Holwerda et al. (2005, § 4.3).

3.1. *Galactic Extinction*

A difference in dust extinction from our own Galaxy between the reference fields (HDF-N/S) and the pointing at the foreground galaxy introduces a bias in the extinction measurement of the specific disk. González et al. (1999) used galaxy counts to measure the extinction toward GRB 970228 and found excellent agreement with other measurements of Galactic extinction (Burstein & Heiles 1978; Schlegel et al. 1998). Schlegel et al. (1998) produced an all-sky map of Galactic extinction based on *COBE* and *IRAS* maps, and we use their values for Galactic extinction (Table 2). Most galaxies in the sample do not show a significant difference in Galactic extinction compared with the average of Galactic extinction toward the HDF-N/S ($A_I = 0.039$ mag). However, the numbers of galaxies from each science field were nevertheless corrected for the difference in Galactic extinction using equation (1).

4. RADIAL OPACITY MEASUREMENTS IN INDIVIDUAL WFPC2 FIELDS

González et al. (1998) presented results based on the SFM for individual WF chips, characterized as "arm" or "disk" regions according to predominance in the chip. Holwerda et al. (2005) segmented the WFPC2 mosaics on the basis of morphological component (arm, interarm, disk) or projected radius from the center. However, the statistics from individual WFPC2 fields barely allow any meaningful opacity measurements for solid angles smaller than a single WF field. In Table 3 we present opacity values for the projected radial annuli in each foreground galaxy in our sample. The radii are expressed in R_{25}, half the D_{25} from RC3. The error bars are computed from the uncertainties in the numbers of real and simulated field galaxies from counting and clustering (Holwerda et al. 2005). For the galaxies for which we have two WFPC2 pointings (NGC 5194, 3621, and 4414), the radial extinction from the combined counts is also shown.

5. AVERAGE RADIAL OPACITY PLOTS

Estimates of extinction in a galaxy disk based on a single WFPC2 chip suffer from poor statistics (González et al. 1998; Holwerda et al. 2005), which makes a radial dependence hard to establish (see Table 3 and Holwerda et al. 2005). This led us to apply the SFM to a large sample of foreground galaxies in order to estimate the general extinction properties of galaxy disks from the combined numbers of field galaxies seen through these disks. We caution against averaging the values in Table 3 to derive average profiles. Figure 2 shows the radial opacity plot from all our fields combined. The numbers of field galaxies from both the science fields and the simulations from all fields were combined on the basis of their projected radial distance from the respective galaxy's centers,[5] expressed in R_{25}. The top

[5] The values used to deproject the distances on the sky to radial distance to the galaxy's center are presented in Table 2.

TABLE 3

RADIAL EXTINCTION PER FIELD

GALAXY	R/R_{25}										
	0–0.25	0.25–0.5	0.5–0.75	0.75–1.0	1.0–1.25	1.25–1.5	1.5–1.75	1.75–2.0	2.0–2.25	2.25–2.5	2.5–2.75
NGC 925	$-0.1^{+1.7}_{-1.5}$	$-0.7^{+0.6}_{-0.6}$	$-0.4^{+0.5}_{-0.5}$	$1.1^{+1.1}_{-1.4}$	...	...	...	...	...	...	...
NGC 1365	...	$0.8^{+0.6}_{-0.6}$	$0.3^{+0.4}_{-0.4}$	...	...	...	...	...	...	...	...
NGC 1425	...	...	$0.8^{+1.1}_{-1.2}$	$1.1^{+0.7}_{-0.7}$	$0.1^{+0.4}_{-0.4}$	$0.6^{+0.6}_{-0.6}$	$0.6^{+1.1}_{-1.4}$	...	...	...	...
NGC 1637	...	$2.9^{+1.6}_{-2.0}$	$2.2^{+1.2}_{-1.6}$	$1.1^{+1.1}_{-1.2}$	$0.5^{+1.1}_{-1.2}$	...	...	...	...	...	...
NGC 2541	$2.2^{+1.7}_{-2.4}$	$0.6^{+0.8}_{-0.9}$	$1.0^{+0.6}_{-0.6}$	$0.4^{+0.4}_{-0.5}$	$1151.0^{+0.4}_{-0.2}$	...	...	...	...	...	...
NGC 2841	$-0.3^{+3.5}_{-3.0}$	$1.3^{+1.0}_{-1.2}$	$1.9^{+1.0}_{-1.2}$	$-0.3^{+0.9}_{-0.9}$	$-0.5^{+1.8}_{-1.5}$	...	...	...	...	...	...
NGC 3031	$1.7^{+0.9}_{-1.1}$	$0.7^{+0.9}_{-1.0}$	...	...	...	...	...	...	...	...	...
NGC 3198	...	$1.6^{+0.9}_{-1.0}$	$0.4^{+0.5}_{-0.5}$	$0.9^{+0.7}_{-0.7}$	...	...	...	...	...	...	...
NGC 3319	$1.5^{+1.2}_{-1.4}$	$1.7^{+0.9}_{-1.1}$	$0.5^{+0.5}_{-0.5}$	$-0.3^{+1.6}_{-1.5}$	...	...	...	...	...	...	...
NGC 3351		$0.6^{+0.9}_{-1.1}$	$0.7^{+1.2}_{-1.9}$	$1715.0^{+0.6}_{-0.4}$	$0.8^{+1.5}_{-1.7}$	$-0.1^{+0.8}_{-0.8}$	$3.0^{+2.0}_{-3.8}$	$0.9^{+1.4}_{-1.7}$	...	$0.0^{+3.0}_{-3.0}$	...
NGC 3621	$-0.3^{+3.7}_{-3.0}$	$1.6^{+0.5}_{-0.5}$	$0.9^{+0.6}_{-0.7}$	...	...	...	...	...	...	...	...
NGC 3621-1	...	$2.2^{+0.7}_{-0.7}$	...	...	...	...	...	...	...	...	...
NGC 3621-2	$-0.3^{+3.7}_{-3.0}$	$1.2^{+0.5}_{-0.5}$	$0.7^{+0.6}_{-0.6}$	...	...	...	...	...	...	...	...
NGC 3627	...	$3.2^{+1.4}_{-1.6}$	$1.1^{+0.7}_{-0.8}$	...	...	...	...	...	...	...	...
NGC 4321	...	$1.2^{+1.4}_{-1.6}$	$3.1^{+1.4}_{-1.8}$	$2.7^{+1.4}_{-2.1}$	...	...	...	...	...	...	...
NGC 4414	...	$0.4^{+1.6}_{-1.7}$	$2.1^{+1.0}_{-1.1}$	$0.3^{+0.4}_{-0.4}$	$1.1^{+0.6}_{-0.7}$	$0.6^{+0.8}_{-0.9}$	...	...	...	...	...
NGC 4414-1	...	$0.2^{+2.3}_{-2.4}$	$4.8^{+2.5}_{-4.9}$	$0.1^{+0.6}_{-0.6}$	$2.7^{+1.7}_{-3.2}$	$0.2^{+1.0}_{-1.1}$	...	...	...	...	...
NGC 4414-2	...	$0.6^{+2.2}_{-2.4}$	$1.2^{+1.1}_{-1.2}$	$0.5^{+0.6}_{-0.6}$	$0.7^{+0.6}_{-0.7}$	$1.1^{+1.4}_{-1.9}$	...	...	...	...	...
NGC 4496A	...	$5.1^{+2.0}_{-2.2}$	$1.0^{+0.7}_{-0.7}$	$1.1^{+1.3}_{-1.6}$	...	...	...	...	...	...	...
NGC 4527	$2.8^{+4.4}_{-7.1}$	$5.7^{+2.9}_{-5.5}$	$2.1^{+1.0}_{-1.0}$	$0.4^{+0.4}_{-0.5}$	...	...	...	...	...	...	...
NGC 4535	$-0.6^{+1.1}_{-0.8}$	$1.4^{+1.1}_{-1.3}$	$1.2^{+0.9}_{-1.0}$	$0.6^{+0.5}_{-0.5}$	$-0.2^{+1.6}_{-1.6}$	...	...	...	...	...	...
NGC 4536	...	$0.0^{+0.6}_{-0.5}$	$1.0^{+0.6}_{-0.6}$	$0.9^{+0.6}_{-0.7}$	...	...	...	...	...	...	...
NGC 4548 (M98)	...	$-4.2^{+26.1}_{-13.6}$	$-0.1^{+0.7}_{-0.7}$	$2.6^{+1.5}_{-2.3}$	$1.1^{+1.1}_{-1.2}$	$0.9^{+0.9}_{-1.0}$	$0.9^{+1.4}_{-1.5}$	$0.9^{+1.0}_{-1.1}$	$0.6^{+0.7}_{-0.8}$	$-1.0^{+1.6}_{-1.2}$	...
NGC 4559	$0.4^{+1.0}_{-1.1}$	$0.0^{+0.6}_{-0.6}$	$0.3^{+0.4}_{-0.5}$	$-1.0^{+1.4}_{-1.0}$	...	...	...	...	...	...	...
NGC 4571	$2.8^{+2.0}_{-2.7}$	$1.4^{+0.7}_{-0.8}$	$0.9^{+0.7}_{-0.7}$	$1.1^{+0.8}_{-1.0}$	...	...	...	...	...	...	...
NGC 4603	$3.6^{+1.1}_{-1.3}$	$0.8^{+0.5}_{-0.5}$	$0.3^{+0.7}_{-0.8}$	...	...	...	...	...	...	...	...
NGC 4639	$9.4^{+3.6}_{-5.7}$	$0.3^{+0.5}_{-0.5}$	$0.5^{+0.5}_{-0.5}$	$-0.2^{+1.0}_{-1.0}$	...	...	...	...	...	...	...
NGC 4725	...	$1.5^{+1.7}_{-2.9}$	$0.8^{+0.5}_{-0.6}$	$0.7^{+0.5}_{-0.5}$	...	...	...	...	...	...	...
NGC 5194	...	$1.4^{+1.0}_{-1.1}$	$1.3^{+0.6}_{-0.6}$	$0.8^{+1.0}_{-1.2}$	...	...	...	...	...	...	...
NGC 5194-1	...	$1.3^{+1.1}_{-1.3}$	$1.0^{+1.0}_{-1.1}$	$1.0^{+1.1}_{-1.4}$	...	...	...	...	...	...	...
NGC 5194-2	...	$1.4^{+1.6}_{-1.8}$	$1.5^{+0.7}_{-0.8}$	$0.8^{+13.2}_{-14.5}$	...	...	...	...	...	...	...
NGC 6946	...	$1.4^{+1.5}_{-2.0}$	$1.8^{+1.2}_{-1.6}$	$-0.1^{+1.0}_{-1.0}$	$2.1^{+1.3}_{-2.0}$	...	...	...	...	...	...
NGC 7331	...	$0.3^{+0.8}_{-0.8}$	$0.2^{+0.4}_{-0.4}$	$1.0^{+0.7}_{-0.8}$	...	...	...	...	...	...	...
UGC 2302	$0.5^{+1.0}_{-1.1}$	$0.5^{+0.6}_{-0.6}$	$0.6^{+0.4}_{-0.4}$	$1.2^{+1.3}_{-1.6}$	...	...	...	...	...	...	...
UGC 6614	...	...	$0.4^{+2.0}_{-2.5}$	$0.6^{+0.9}_{-1.2}$	$0.6^{+1.1}_{-1.2}$	$0.5^{+1.1}_{-1.2}$	$-0.6^{+0.8}_{-0.8}$	$-0.3^{+0.7}_{-0.7}$	$0.2^{+0.7}_{-0.7}$	$0.6^{+0.6}_{-0.7}$	$0.5^{+0.7}_{-0.7}$

NOTE.—The individual radial extinction measurements (in magnitudes) of the galaxies in our sample based on the field galaxy counts. Note that the intrinsic uncertainty in the background field of galaxies keeps the error in these measurements high. The counts have been corrected for the difference in Galactic extinction between the target foreground galaxy and the average of the HDF fields. These values are *not* corrected for inclination in any way. UGC 6614 has the largest radial coverage because of its extreme distance; in addition to the values shown, UGC 6614 has an extinction measurement for the radial interval between 2.75 and 3 R_{25} of $0.8^{+1.2}_{-1.3}$. The averages presented in the rest of the paper are the result of combining the numbers of background galaxies, and we caution against averaging these values to get a profile for a subset of the sample.

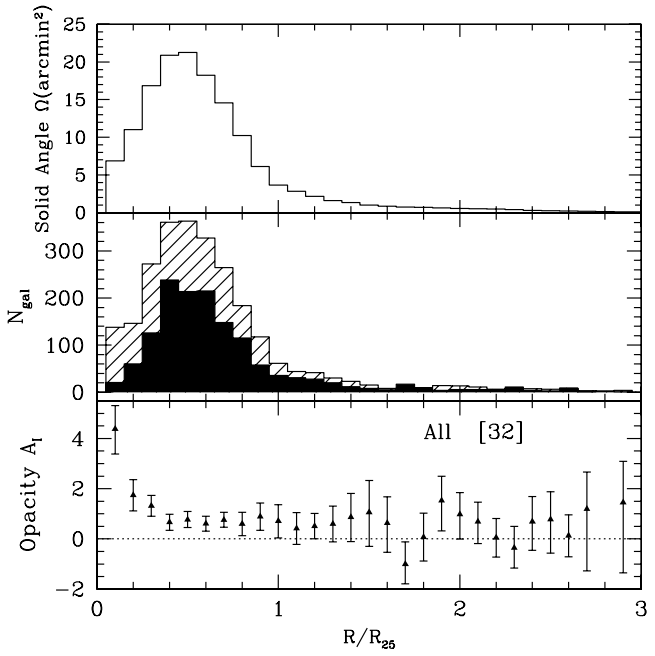

FIG. 2.—Composite of our entire sample (32 WFPC2 fields). The top panel shows the total solid angle in each annulus as a function of scaled radius. The number of field galaxies found (*middle*) is presented for both the synthetic fields without dimming (*shaded histogram*) and the science fields (*filled histogram*). The bottom panel shows the derived opacity in each annulus as a function of radius. No inclination correction has been applied to these results.

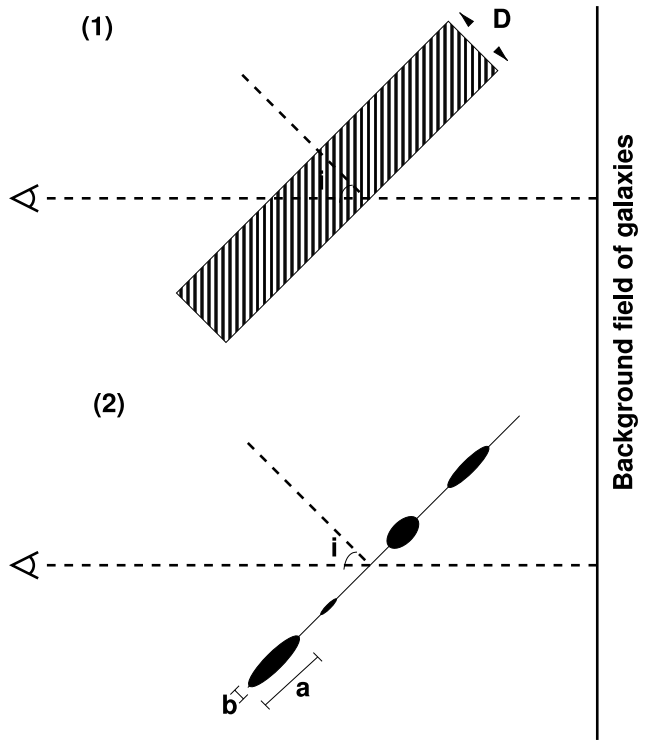

FIG. 3.—Two models of dust geometry in the disk. The flat screen with a thickness D (1) and the screen of dark clouds (2). See the text for the effect of the thick screen. The effect of oblong clouds depends on the observed filling factor of the clouds. The observed optical depth (τ) is related to the filling factor by $\tau = \ln(1-f)$. The observed filling factor is related to the face-on value as follows in case of the oblong clouds: $f = \epsilon f_{\rm obs} + (1-\epsilon)\cos(i) f_{\rm obs}$. From the relation between opacity and optical depth [$A = -2.5\log(e^{-\tau})$, eq. (1) ($A = -2.5\log(N/N_0)$] and these expressions for the filling factor, eq. (3) can be derived. The average oblateness [$\epsilon = 1 - (b/a)$] of the clouds influences directly the inclination correction. If they are spherical ($\epsilon = 0$), then the effect of inclination on the number of field galaxies is most profound. However, if they are effectively flat ($\epsilon = 1$), then there is no effect of inclination on the numbers (the projection effects on the effective cloud size and filling factor cancel each other).

panel in Figure 2 shows the total combined solid angle for each radial bin for which the average opacity was determined. The middle panel shows the number of field galaxies from the science field and the average number found in the simulations without any dimming ($A = 0$). The bottom panel shows the opacity for each bin derived from the intersection of equation (1) fitted to the simulations and the real number of galaxies.

The solid angle or the number of simulated galaxies without any dimming is a good indicator for the reliability of our opacity estimate, as reflected by the error bars in the bottom panel of Figure 2. The estimates are limited at small radii by the high surface brightness and crowding of the foreground galaxy center, effectively masking some of the solid angle available at those radii. At higher radii the uncertainty comes from too little of the solid angle being covered (see Fig. 2, *top*). This is a selection effect of our sample, as most of the WFPC2 fields were pointed at the optical disk of the galaxy.

To determine the effects on average radial opacity of disk inclination, prominence of spiral arms, or Hubble type, radial opacity plots of subsets of our sample were constructed. The solid angle used is then some fraction of those in the top panel in Figure 2, which consequently increases the uncertainty in the opacity measurement. To counter this problem, radial binning of 0.2 R_{25}, instead of 0.1 R_{25} (Fig. 2), was applied.

5.1. *Inclination Effects*

The inclination of foreground disks affects measured opacity, but the amount of this effect depends on dust geometry. In the case of a uniform thick screen, the path length attenuating the field galaxies is increased. However, in the case of a screen of dark clouds in the disk, the effect is on the apparent filling factor of clouds. Because the correction depends on which dust geometry is assumed, we present the radial results (Fig. 2) without any correction and explore corrections using several different models, as illustrated in Figure 3. The homogeneous screen results in a multiplicative factor cos i to be applied to the opacity value (A) or in a correction to the number of field galaxies found in the science field, as follows:

$$N_\perp = \frac{N_i^{\cos i}}{N_0^{\cos i - 1}}. \qquad (2)$$

The other models consider a screen with fully opaque clouds or patches. Depending on the thickness of these clouds, the apparent filling factor depends differently on inclination. In these models the clouds have an average oblateness ϵ [$\epsilon = 1 - (b/a)$] with major axis a and minor axis b of the clouds. Following the geometry of Figure 3, the relation between the number of field galaxies, seen through the foreground disk face-on ($N_\perp$), at an inclination i (N_i), and the average number of field galaxies in the field behind the foreground galaxy (N_0) can then be expressed as

$$N_\perp = (1-\epsilon)(1-\cos i)N_0 + [\epsilon(1-\cos i) + \cos i]N_i, \qquad (3)$$

where the extreme cases for ϵ are spherical clouds ($\epsilon = 0$) and flat patches ($\epsilon = 1$). The oblateness ϵ parameterizes the ratio between the scale height of the dust and its extent in the plane of the disk. In images of edge-on disks, the visible dust lanes are

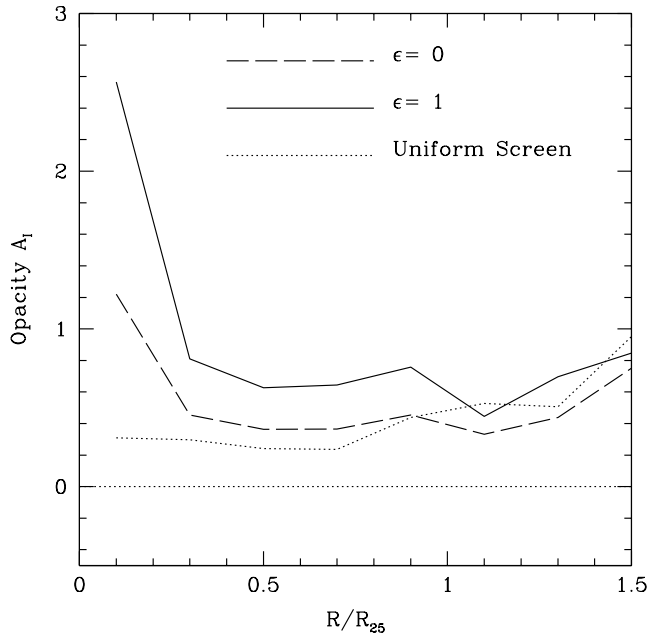

FIG. 4.—Average opacity as a function of radius, derived from the number of field galaxies corrected for inclination with eq. (2). Flat clouds ($\epsilon = 1$) do not influence the numbers. The maximum correction ($\epsilon = 0$) has the largest effect on high opacities. The opacity profile from the number of field galaxies corrected for inclination using a smooth screen is also shown.

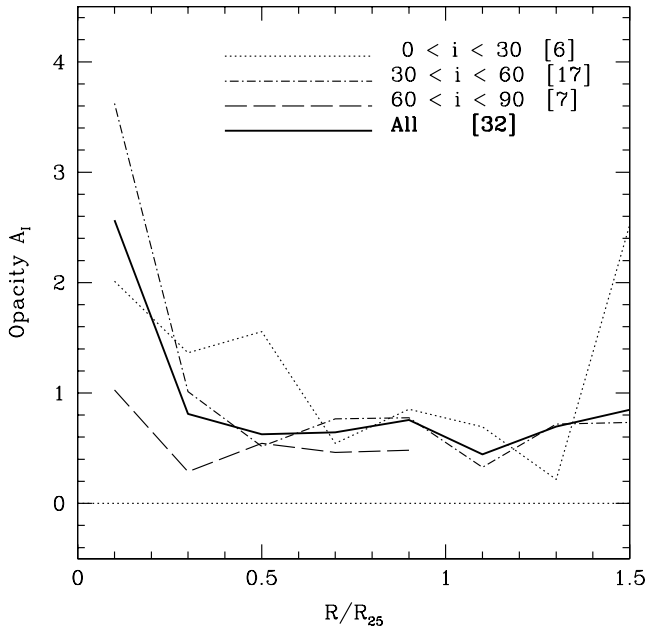

FIG. 5.—Average opacity as a function of radius, taken over our entire sample (*thick line*) and four subsets based on inclination. The number between brackets denotes the number of fields in each bin. As there is not discernible trend with inclination, other effects must dominate the average opacity. For this reason we choose to ignore the effects of inclination on our measurements. Beyond 1.3 R_{25}, the values are from poor statistics, which explains the occasional negative value.

confined to a thinner disk than the stars. It is therefore likely that ϵ is not 0. For purposes of illustration we use a value of 0.5 in Figure 8.

Figure 4 shows the radial profile from Figure 2 corrected for both extreme cases and uniform screens in all galaxies. The contributions from each galaxy to the composite radial profile were corrected according to equations (2) and (3) before addition. Figure 5 shows the total uncorrected radial profile for four subdivisions of our sample based on inclination. From Figure 5 it seems clear that other effects are much more important than the inclination of the foreground disk. For this reason we ignore the effects of inclination on our measurements. As the effects of inclination are debatable on the basis of preferred dust geometry, we present further results without inclination corrections, except where noted.

5.2. *The Effect of Spiral Arms*

Another effect on the average radial opacity profile in Figure 2 is due to the presence of spiral arms. Because our sample is predominantly from the Cepheid Distance Project, the WFPC2 images all feature spiral arms. If these are more opaque than the disk proper (Beckman et al. 1996; White et al. 2000), then the radial profile presented in Figure 2 could be biased toward higher opacities. Separate radial plots for the arm, the interarm part of the disk, and outside any spiral arm part of the disk are shown in Figure 7 based on the counts from the typical regions in the entire sample, with the exception of the low surface brightness (LSB) galaxies UGC 2302 and UGC 6614. They were left out because not much spiral structure can be discerned; they appear completely transparent (see Fig. 8).

5.2.1. *Segmenting Images*

To differentiate between the effects of spiral arms and disks in the opacity plots, the images were segmented into crowded, arm, disk (interarm), and disk (outside arm). These regions were flagged in the mosaicked WFPC2 fields using the GIPSY function *blot*, in the same way as NGC 1365 in Holwerda et al. (2005). The choice of typical regions was made in order to compare the arm and interarm results of White et al. (2000) and Domingue et al. (2000). A typical mask is presented in Figure 6, and masks for all galaxies in the sample are presented in Holwerda (2005). It should be noted that this segmentation into typical regions is subjective and is based on those sections of the foreground galaxies covered by the WFPC2 observations we use.

5.2.2. *Radial Extinction for Typical Disk Regions*

Radial extinction profiles of the typical regions are presented in Figure 7. The arm regions show much more opacity and a much more pronounced radial dependence of that opacity. There is a radial dependence as well for the interarm parts of the disk, although it is not as steep. The outside parts of the disk of the spiral galaxy, however, show little or no relation between opacity and radius. The opaque components of a spiral disk appear to be the spiral arms, while the disk itself is more transparent but much more extended. Figure 7 also shows the total solid angle of the radial annuli over which the opacities are determined. From these we can conclude that the regions deemed "arm" do not dominate the whole of the fields. The radial effect of the arms only becomes visible in the total radial opacity plot (Fig. 2 and Fig. 7, *top left*), at the lower radii where the arms and the interarm region dominate. In Figure 8 we present the profiles corrected for inclination assuming an ϵ of 0.5. The general trends remain but now for somewhat lower opacity values.

5.2.3. *Comparison with the Occulting Galaxy Method*

White et al. (2000) and Domingue et al. (2000) presented their extinction values from occulting galaxy pairs as a function of the radius, scaled with R_{25}. White et al. (2000) compared ground-based photometry, and Domingue et al. (2000)

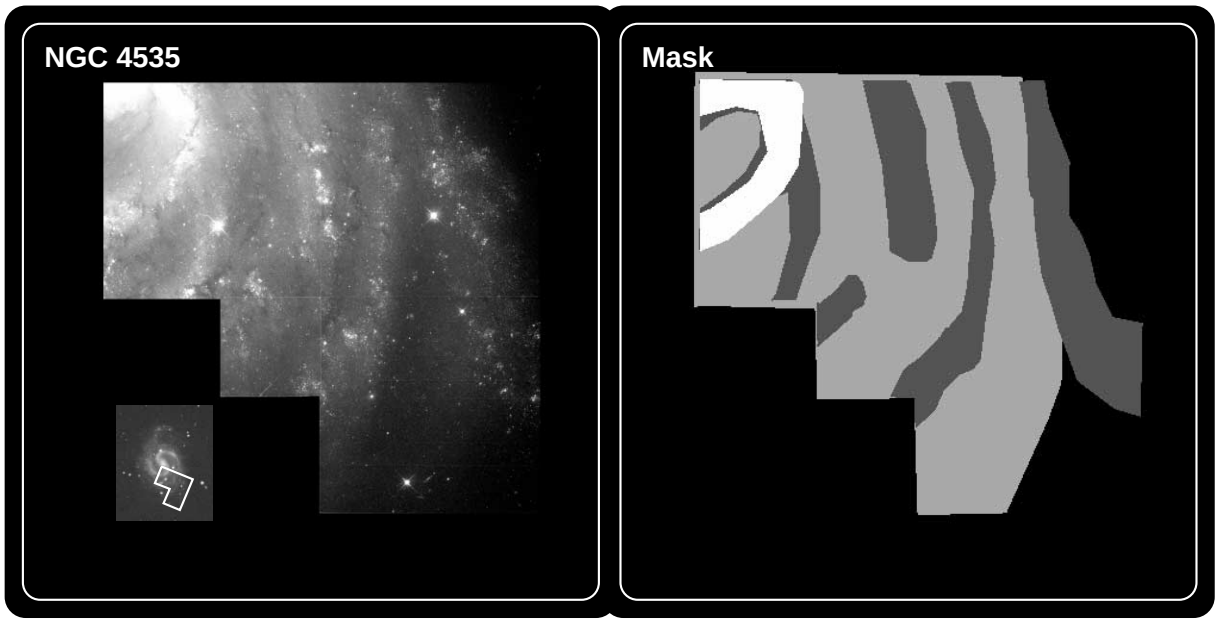

FIG. 6.—Mask of typical regions for NGC 4535. White regions represent "crowded" regions, dark gray are "arm" regions, light gray interarm disk regions, and all objects not in any of the above categories are outside disk region.

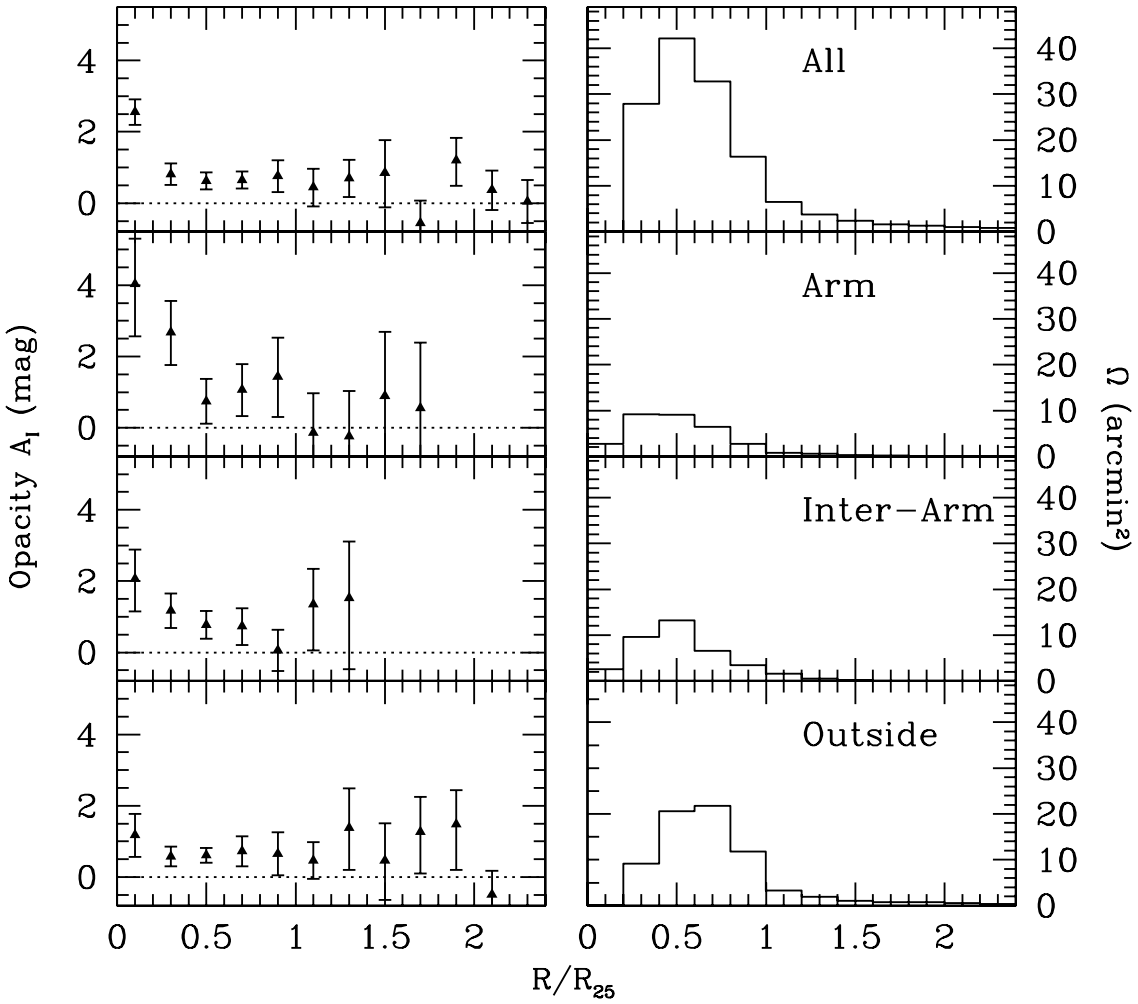

FIG. 7.—Average opacity as a function of radius (*left*), taken over our entire sample for each of three typical regions in the spiral disk: arm regions, disk regions enclosed by spiral arms (interarm), and disk regions not enclosed by spiral arms (outside). The right panels show the solid angle as a function of radius.

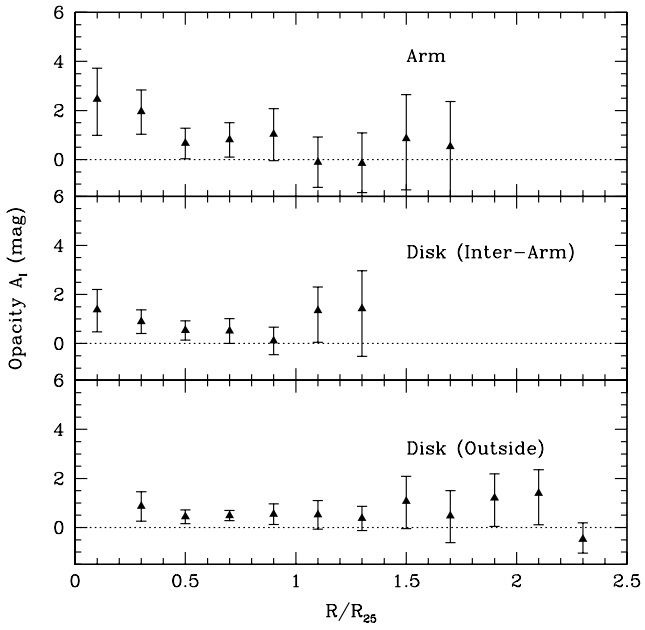

FIG. 8.—Same as Fig. 7, but the numbers of galaxies from the science fields were corrected for inclination using eq. (2) and $\epsilon = 0.5$.

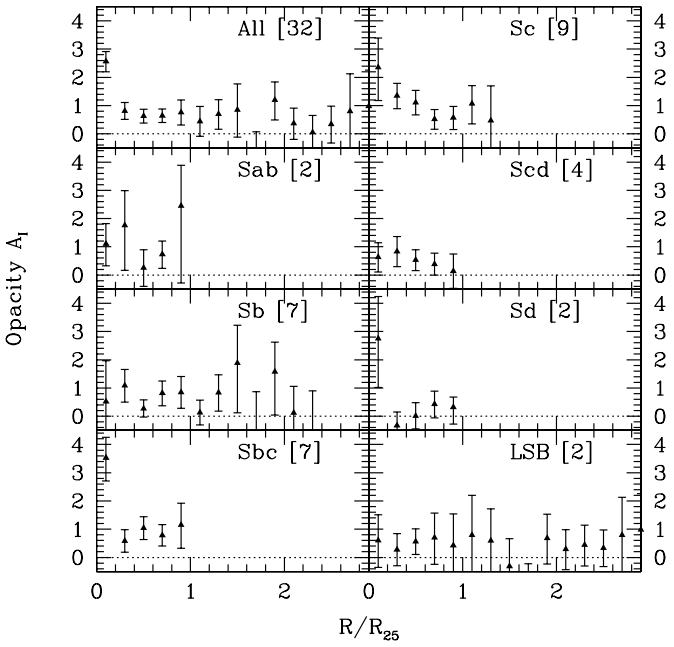

FIG. 10.—Average opacity as a function of radius, taken over our entire sample (*top left*) and for all Hubble types in our sample. LSB galaxies are treated as a separate Hubble type. UGC 6614 is the most distant galaxy in our sample (with the smallest R_{25}), and hence the wide coverage in radius for the LSB galaxies but with large uncertainties for the opacities. The number between brackets is the number of WFPC2 fields averaged for each plot.

used spectroscopic measurements of the occulted galaxy light. These extinction points are plotted in Figure 9 for arm and interarm regions. The extinction curves from Figure 7 and the inclination-corrected curve from Figure 8 are plotted as well. Both the arm and the interarm extinction values as a function of radius agree well with the values obtained from the occulting galaxy technique. It is remarkable how well the results compare, considering they were obtained from completely different samples of spiral galaxies and using different techniques. The values from the occulting galaxy technique are slightly lower than ours. There are several possible reasons for this. It is possible that the spectroscopic results from Domingue et al. (2000) (Fig. 9, *triangles*) favor the more transparent regions in a disk (D. L. Domingue 2004, private communication). But, more importantly, the sample of occulting foreground galaxies consists of a different makeup of spiral galaxy subtypes than that of this paper. It should be noted that there are no galaxies common to both our sample and that of the occulting galaxy technique. Domingue et al. (2000) noted that their later types (Sbc) seem more opaque, as do we (Fig. 10). Figure 11 compares the results for the most prevalent Hubble subtypes in the occulting galaxy method (Sb and Sbc) with our results for them. The arm values seem to match up, but there is a difference in the interarm results. It is unclear to us whether this points to a structural effect in either technique. A likely explanation is that the definition of "interarm" applies to slightly different regions in the spiral disks for White et al. (2000), Domingue et al. (2000), and this paper. This paper's definition of typical regions is based on the high-resolution mosaic, whereas the White et al. (2000) is derived from their ground-based imaging. It is therefore possible that we include sections in the interarm regions that the occulting techniques would not resolve as interarm, increasing our values of opacity for those regions with respect to the occulting galaxy technique.

The SFM provides an independent verification of the occulting galaxy technique using a fundamentally different approach. In addition, a component was added to the distinction between arm and interarm parts of the disk, namely, the outside, meaning not directly enclosed by spiral arms. The fact that this component is not fully transparent raises the possibility of a dust disk extending beyond the spiral arms (Fig. 8).

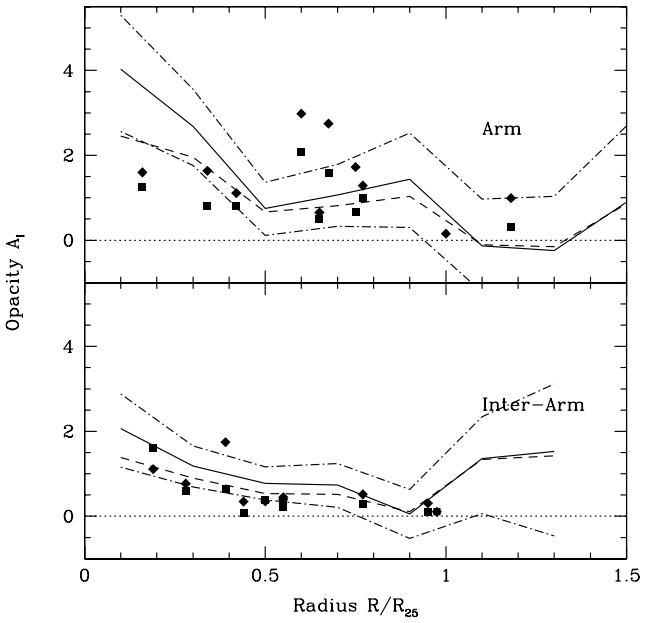

FIG. 9.—Radial extinction profile from the counts of field galaxies (*lines*) and the occulting galaxy technique (*points*). The top panel shows the "arm" regions, the bottom the interarm regions. The solid line is the SFM extinction profile uncorrected for inclination, with the uncertainty denoted by the dot-dashed lines. The dashed line shows the opacity corrected using $\epsilon = 0.5$. The filled squares and diamonds are the A_I and A_B from White et al. (2000), respectively, and the triangles are the opacities from Domingue et al. (2000). All symbols are uncorrected for inclination. Typical uncertainties for these are of the order of a couple of tenths of magnitude.

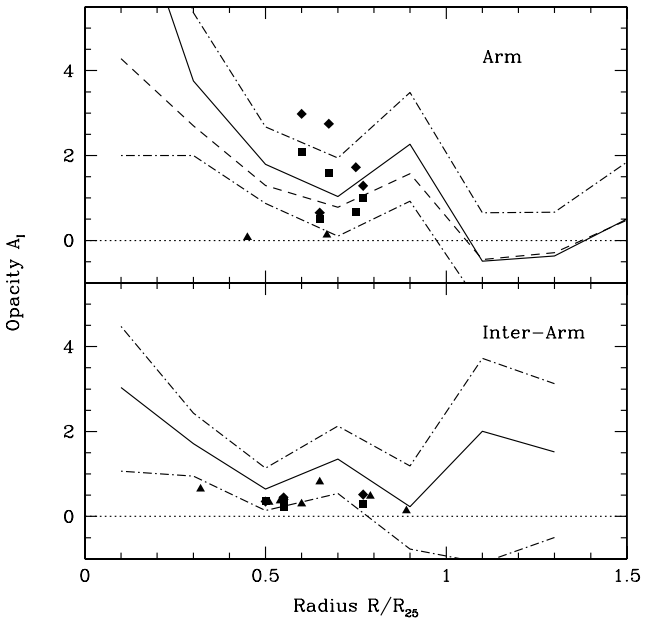

FIG. 11.—Radial extinction profile from the counts of field galaxies and the occulting galaxy technique (the lines and points are as in Fig. 9) for the spiral galaxy Hubble subtypes that both techniques have in common, the Sb and Sbc galaxies. Points in Fig. 9 without a spiral galaxy subtype noted in White et al. (2000) and Domingue et al. (2000) are omitted. Lines are the same as in Fig. 9.

5.3. *Hubble Type*

With the effect of spiral arms on the opacity profile, the Hubble type is likely to have an influence on the profile. Figure 11 shows the extinction profiles averaged per Hubble type. Hubble types Sab through Sd are presented, as well as the average opacity profile of the two LSB galaxies in our sample. Hubble types Sab through Scd in our sample show disk extinction up to R_{25}. The Sab result is tentative, because of the poor statistics from only two WFPC2 fields. The Sd and LSB galaxies, however, appear effectively transparent. LSB galaxies were in fact assumed to be transparent by O'Neil et al. (2000) when they discussed the morphology of field galaxies seen though them. However, both profiles, Sd and LSB, are based on only two WFPC2 fields, which accounts for the higher uncertainties. When we compare early-type galaxies with later types, it appears that the later type galaxies (Sbc–Sc) show more extinction and do so at larger radii. The Sb galaxies show a bump that appears to be associated with higher extinction from the more tightly wound spiral arms.

Figures 12 and 13 show the radial profiles for arm and disk—both interarm and outside regions—for our sample divided into early and late spiral galaxies. A finer separation in Hubble type would have resulted in even higher uncertainties, because of the lack of solid angle and hence statistics. The solid angle of each radial annulus is also plotted. Purely arm regions do not dominate the opacity profiles. However, the interarm regions are similar

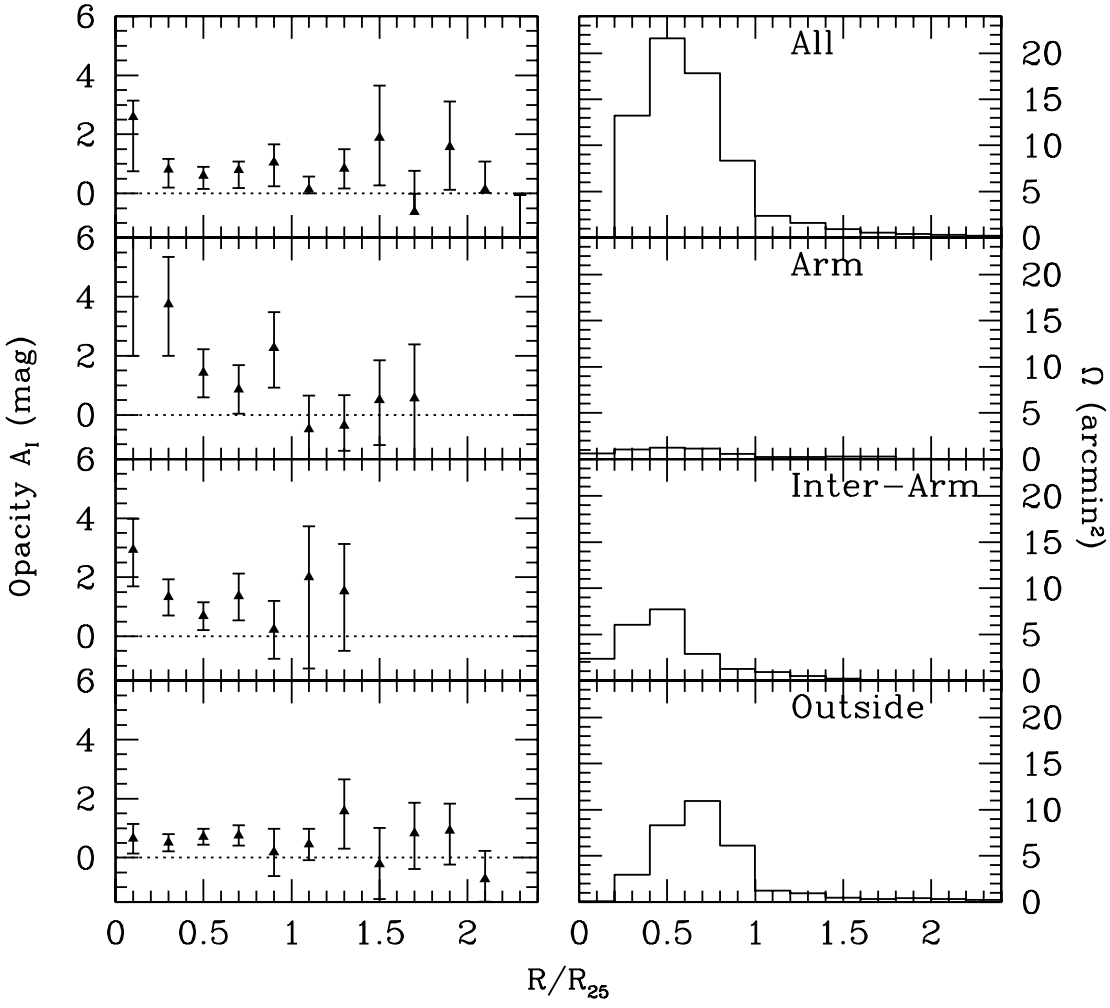

FIG. 12.—Average opacity as a function of radius, taken over the early spiral galaxies (Sab, Sb, and Sbc) in our sample, for each of three typical regions in the spiral disk: arm regions, disk regions enclosed by spiral arms (interarm), and disk regions not enclosed by spiral arms (outside).

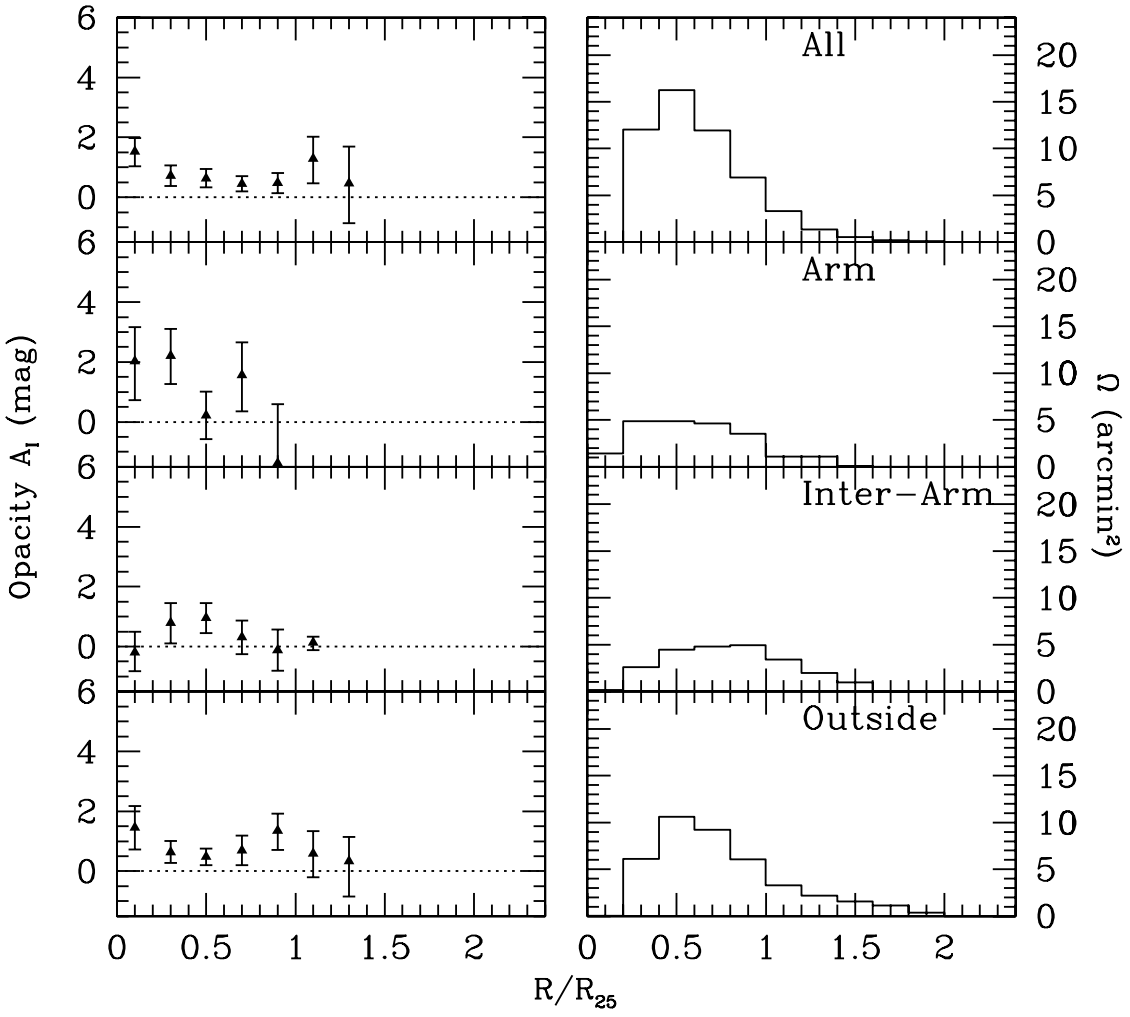

FIG. 13.—Average opacity as a function of radius, taken over the late spiral galaxies (Sc, Scd, and Sd) in our sample, for each of three typical regions in the spiral disk: arm regions, disk regions enclosed by spiral arms (interarm), and disk regions not enclosed by spiral arms (outside).

in behavior (Figs. 7 and 8). The inner parts of the profile are therefore more armlike, while the remainder is disk dominated.

The radial dependence of arm and interarm regions is more pronounced in the case of earlier galaxies than for later types. The opacity in the spiral arms is substantially higher than in the disk, for both early and late types. The total profiles show bumps at 0.9 and 1.1 R_{25} for the early and late types, respectively. In the case of the early types this seems due to the spiral arm contribution at that radius. The bump for the late types is not as significant, but it might be related to the general position of spiral arms as well.

6. AVERAGE COLOR OF THE FIELD GALAXIES

The average color of the field galaxies found in the science fields can in principle tell us something about the actual dust geometry responsible for the drop in numbers. If there is a correlation between the average reddening of the field galaxies and the average opacity of the foreground spiral, then the dust extinction responsible for the drop in number of field galaxies is, at least in part, in the form of a diffuse screen, reddening the visible galaxies. If, however, the average color of the field galaxies does not change with opacity, then the drop in their number is likely due to fully opaque clouds with transparent sections between them to allow for the detection of the unreddened surviving field galaxies.

Our method influences the average color of the detected field galaxies in several ways. The V band (F555W) for the synthetic field background was constructed from the original HDF images in the F606W and F450W filters. However, González et al. (1998) estimated that this introduces a negligible error. Crowding introduces blended objects in the synthetic fields. The synthetic counts are corrected for this effect, but it does influence the average color. The simulated dust extinction we used was gray, so no preferred reddening was introduced in the synthetic fields. However, our automated selection procedure for field galaxy candidates selects against very blue objects, introducing a preference for red galaxies. A similar selection effect may take place in the visual check of the science fields, as blue objects are treated as suspected foreground objects. Overall, these selection biases cause the average color of the field galaxies in the science and synthetic fields to be redder than the average for an unobstructed field of distant galaxies. The effects of blended objects on the average colors of science and synthetic fields are not identical, as not all blends have been removed from the synthetic counts. Nonetheless, we can compare the trends of both these average colors with radius.

The average $V - I$ color of the field galaxies found in the science fields, the simulation without extinction ($A = 0$), and the opacity derived from the galaxy numbers are plotted as a function of radius in Figure 14. The average $V - I$ color of the field galaxies in the science fields does not change with radius and hence average opacity. The average color of the synthetic field objects appears to become bluer with radius. However, beyond 1.4 R_{25} the number of objects is very small, and the averages should be treated with caution. Comparing the average color of distant galaxies from science and synthetic fields for the inner part of the disk, the average of the science field objects is redder than the synthetic field average. This difference in average color is likely the result of blends with blue foreground objects being inadvertently included in the selection of synthetic field objects. The number of objects from the synthetic fields was corrected for this effect (see also Holwerda et al. 2005), but the average color was not. The science field objects do not suffer from this problem as they were checked visually for blended objects. The field galaxies seen in the science fields are likely visible in parts of the disk that are nearly transparent or, alternatively, the dust screen in the disk behaves according to the "gray" extinction law. This is remarkable, considering the bias toward redder objects throughout our method.

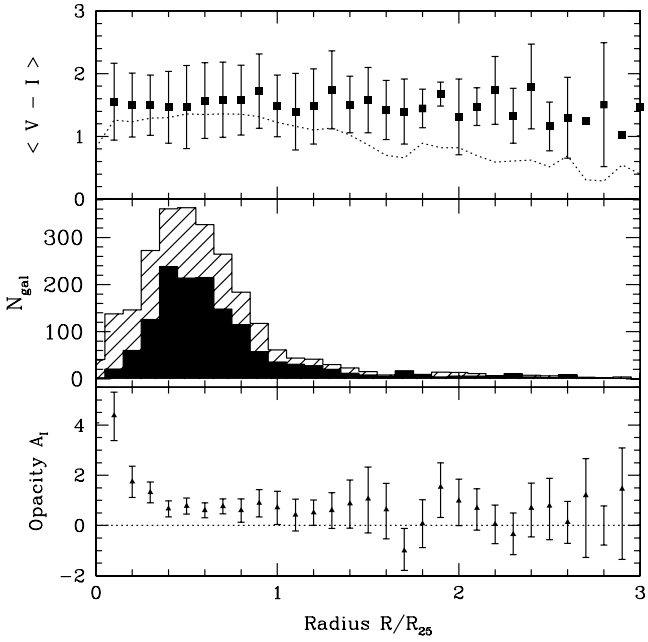

FIG. 14.—Color changes with radius based on the entire sample of 32 WFPC2 exposures. *Top*: Average $V - I$ color of field galaxies found in the science fields as a function of radius. The error bars denote the standard deviation of the distribution of $V - I$ colors. The dotted line is the average of the synthetic field objects. *Middle*: Number of field galaxies found in the simulated fields without extinction (*shaded histogram*) and in the science field (*filled histogram*) as a function of radius. *Bottom*: Opacity derived from the numbers of field galaxies as a function of radius, expressed in R_{25}.

Figure 15 shows the average color-extinction measurements for the field galaxies in the science fields. The Galactic extinction law is shown for comparison. Each point has been determined in a radial annulus for all the fields combined (Fig. 2) and for the typical regions (Fig. 7, but with the finer radial sampling of Fig. 2). Without distinction between regions, no trend with opacity can be discerned for the average color.

The average color in the arm regions does not seem to increase much with opacity. The arm extinction is decidedly gray, something also found by González et al. (1998). For the disk regions, no distinct trend can be seen, and they do not seem to follow the Galactic law very closely. González et al. (1998) found the disk region of NGC 4536 to be more Galactic in its reddening law. There is an average reddening with respect to the average $V - I$ color of the HDF objects identified as galaxies by our algorithm without a foreground disk. This reddening is likely the result of the effects of the visual check and contamination of the color measurement by stray disk light.

These color-extinction relations for both arms and disk seem to be grayer than the Galactic extinction slope, favoring the possibility that at least part of the extinction is in opaque clouds. The uncertainties are such, however, that even for our

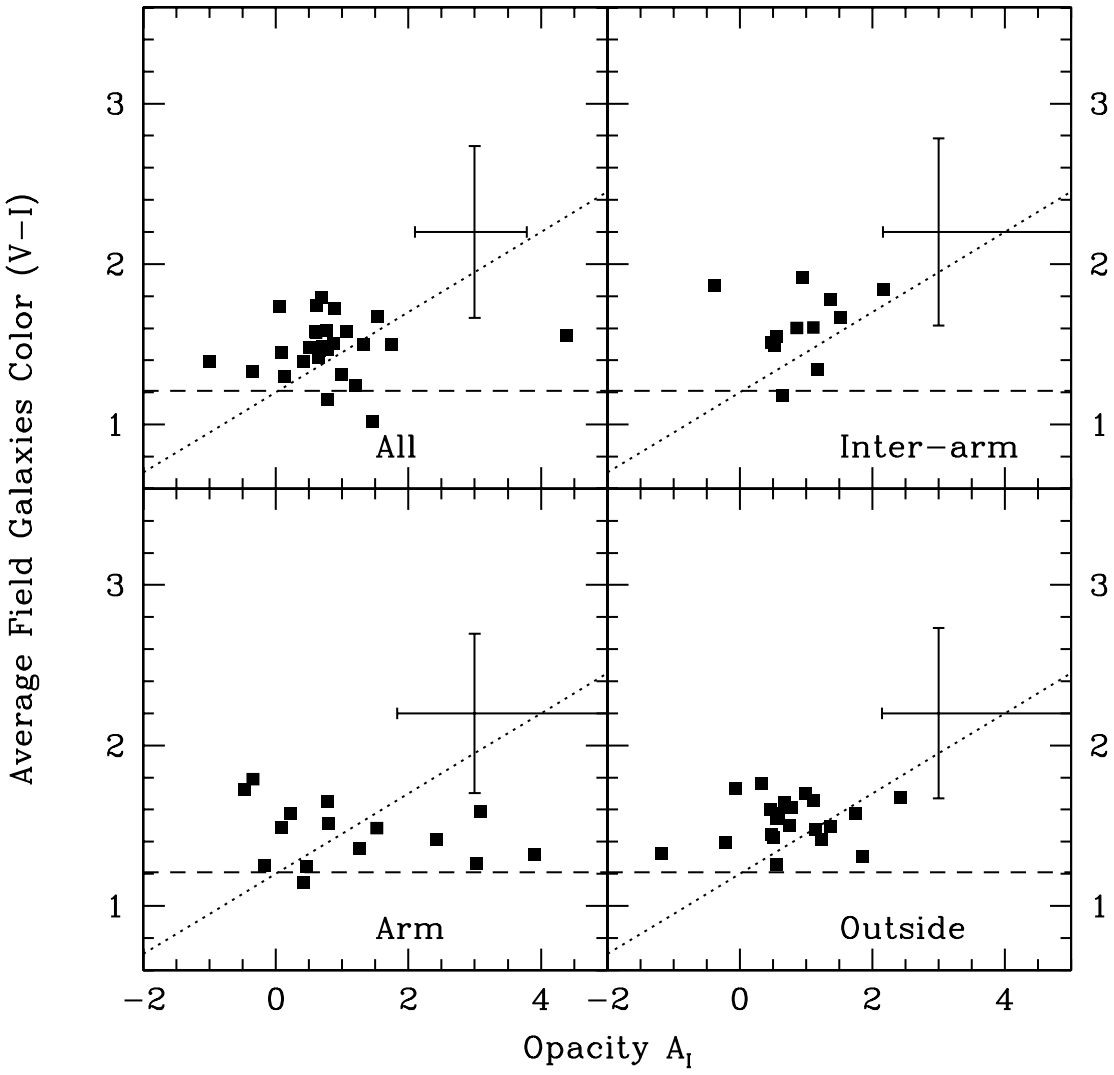

FIG. 15.—Average galaxy color ($V - I$) as a function of average opacity (A_I). The error bars denote the average uncertainty in opacity and average standard deviation in the distribution of colors of field galaxies from the science fields. The dotted line is the Galactic reddening law, normalized to the average color of the HDF galaxies. The dashed line is the average color of the HDF galaxies, identified as such by our algorithm without any foreground field. Selection effects and blends most likely account for the reddening compared with the HDF galaxies.

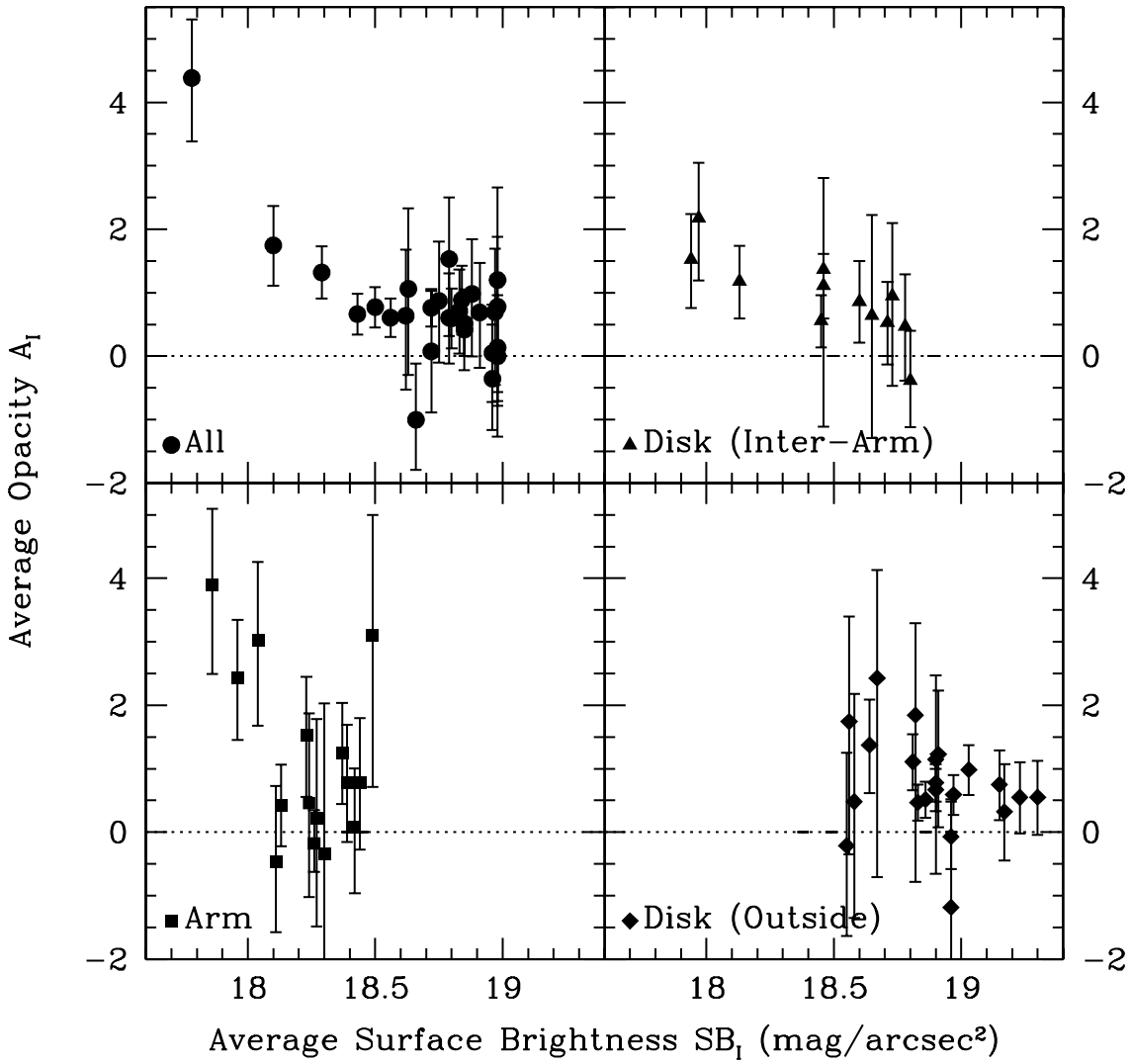

FIG. 16.—Average opacity as a function of average surface brightness. Both surface brightness and opacity were determined from the radial annuli in Fig. 2. In these same annuli the opacity and surface brightness were determined for each typical region. Radial annuli regardless of type of region are the dots. Values from annuli in the arm regions are the squares. Disk values in the interarm and outside regions are the triangles and diamonds, respectively.

increased statistics no good relation between opacity and color can be found.

7. SURFACE BRIGHTNESS AND OPACITY

The counts of distant galaxies were added per radial annulus, expressed in R_{25}. In addition, the flux and solid angle from each field can be added for each radial annulus. The averaged surface brightness (SB_I) and the average opacity (A) from each radial bin in Figure 2 are plotted in Figure 16. These values for the radial bins per typical region in Figure 7 are plotted as well but with finer sampling. There is a hint of a relationship between luminosity and extinction. This is consistent with the relation found by Giovanelli et al. (1995) and Masters et al. (2003) between overall disk opacity and the galaxy's total luminosity. The solid angles over which the surface brightness and opacity were averaged were selected by radius and not luminosity. Areas with different surface brightnesses are therefore combined at each radius, smoothing out any relation between opacity and surface brightness. Hence, most of the points in Figure 15 are around the same opacity, and the range of surface brightness values is small. Nevertheless, the values of high extinction and brightness ($SB_I < 18.5$) do show some relationship between surface brightness and opacity, with arm regions displaying more extinction at the same surface brightness levels than the interarm disk. The disk values appear to show no correlation, but these values are per definition not for high surface brightness levels. And yet, together with the higher values of opacity found for the spiral arms, the points are not inconsistent with a relation between opacity and luminosity. Opacity measurements in partitions of the WFPC2 images based on average surface brightness instead of radius should reveal any relation more clearly. This comparison between extinction and emission will be presented in more detail in a later paper.

8. DISCUSSION

From the number of field galaxies found through the disks of spiral galaxies, a quantitative picture of extinction as a function of radius can be found. The SFM is too limited by poor statistics to obtain a good result for individual fields. However, a meaningful measurement can be derived from a combination of several galaxies. The effect of spiral arms on the radial extinction is quite distinct and dependent on Hubble type. From these radial

plots it becomes clear that the dust in the disk is not one smooth layer sandwiched between the disk's stars, but two separate components: radially dependent spiral arms and a more transparent but also extended disk. In addition, there is a highly opaque central bulge component.

Whether the average opacity is a result of dust clouds or a smooth screen of gray dust is difficult to determine from the numbers, colors, and luminosities of the field galaxies found through the disks of our sample. However, the relative independence on inclination of the average opacity measured from numbers of spiral galaxies and the gray relation between opacity and average field galaxy color both point toward a patchy distribution of the absorbing dust in the disk.

Assuming that the optical depth of the disk can be expressed as $\tau = \ln(1 - f)$, where f is the area filling factor, the average opacity of $A_I \approx 0.5$ would require a filling factor of 40% of the disk, a figure that rises to 85% in the spiral arms. While the visible dust lanes can account for at least a part of these clouds, other dust clouds are likely embedded in the disks and arms. This patchy coverage explains the occasional distant galaxy seen through a spiral disk (Roennback & Shaver 1997; Jablonka et al. 1998), which has sometimes been used as anecdotal evidence for transparent disks. The disk is in fact relatively transparent where background galaxies are seen. However, by calibrating the number of the distant galaxies found, a very different picture emerges.

While this result is consistent with earlier findings, these values are likely upper limits, not lower ones. Any inclination correction would lower the face-on value for extinction. However, the patchy nature of dust extinction is likely responsible for a high variety of extinction values in the disk. Integrated measurements such as light profiles, however, would be affected according to the presented opacity values. A possible relation between extinction and brightness would also cast doubt on the fixed mass-to-light ratios generally assumed when modeling the kinematics of a spiral disk.

9. CONCLUSIONS

The effects of dust extinction on the number of field galaxies found in our fields lead us to the following conclusions:

1. The SFM gives an unbiased but uncertain measure of opacity for single WFPC2 fields (Table 3).
2. On average, the disk of a spiral galaxy has an opacity in I of $\approx$1 mag (Fig. 2).
3. The extinction measured from the number of field galaxies seems to be independent of the inclination of the foreground disk over the range in i covered by our sample ($10^\circ < i < 70^\circ$) (Fig. 5). This is consistent with fully opaque flattened clouds covering a fraction of the area as the cause of the observed average opacity.
4. The absorption profile for typical regions in the disk is strongly influenced by the spiral arms. Spiral arm regions are the most opaque and display a radial dependence. The disk regions enclosed by a spiral arm are also more opaque than other disk regions and display a similar radial dependence (Fig. 7).
5. The radial extinction curves derived from numbers of background galaxies and those reported by the occulting galaxy technique agree reasonably well (Figs. 9 and 11), although a systematic effect in either technique (or both of them) seems to be present in the interarm results (Fig. 11).
6. Sc galaxies show much more opacity in their central regions than other types (Fig. 10).
7. All Hubble types earlier than Scd in our sample show substantial disk extinction in I up to R_{25} (Fig. 10).
8. The numbers from Sd and LSB galaxies are consistent with a transparent disk, but these measurements are limited by statistics. (Fig. 10).
9. Both early- and late-type spiral galaxies exhibit the extinction profiles of the two distinct components: a radially dependent one (arm and interarm) and a more extended disk (outside arms) (Figs. 12 and 13).
10. The average color of the distant galaxies identified in the science fields does not change with either radius or the opacity derived from their numbers (Fig. 14).
11. The gray nature of the absorption derived from field galaxy counts and colors holds for all typical regions (Fig. 15). The absence of inclination effects and the gray nature of the absorption is consistent with strongly absorbing dense clouds masking off the distant galaxies. Their covering factor in the disk would be around 40% regardless of cloud sizes (which our technique cannot provide).
12. The average surface brightness in radial annuli and the corresponding average opacity derived from distant galaxy counts appear correlated. They are consistent with a rise of opacity with surface brightness (Fig. 16). Although the range of surface brightness is small and the uncertainty in opacity rises with higher surface brightness, this is in good agreement with earlier results for bright galaxies. This would constitute a relation between dust mass and light.

The Synthetic Field Method has proven itself to be a useful, model-independent technique for measuring the total opacity of spiral disks. It can be applied to any spiral disk at intermediate distance for which high-resolution imaging is available. We will present further results for opacity as a function of surface brightness in a future paper.

The authors would like to thank the anonymous referee for his or her comments and Harry Ferguson for insightful discussions on the Synthetic Field Method. This research has made use of the NASA/IPAC Extragalactic Database, which is operated by the Jet Propulsion Laboratory, California Institute of Technology, under contract with the National Aeronautics and Space Administration (NASA). This work is primarily based on observations with the NASA/ESA *Hubble Space Telescope*, obtained at the STScI, which is operated by the Association of Universities for Research in Astronomy (AURA), Inc., under NASA contract NAS5-26555. Support for this work was provided by NASA through grant number HST-AR-08360 from STScI. STScI is operated by AURA, Inc., under NASA contract NAS5-26555. We are also grateful for the financial support of the STScI Director's Discretionary Fund (grants 82206 and 82304) and of the Kapteyn Institute of Groningen University.

REFERENCES

Alton, P. B., Bianchi, S., & Davies, J. 2001, Ap&SS, 276, 949
Beckman, J. E., Peletier, R. F., Knapen, J. H., Corradi, R. L. M., & Gentet, L. J. 1996, ApJ, 467, 175
Bovill, M. S., Pritzl, B. J., & Knezek, P. M. 2003, BAAS, 203, 115.10
Burstein, D., & Heiles, C. 1978, ApJ, 225, 40
Cabanac, R. A., de Lapparent, V., & Hickson, P. 2000, A&A, 364, 349
Calzetti, D. 2001, PASP, 113, 1449
Cropper, M., Soria, R., Mushotzky, R. F., Wu, K., Markwardt, C. B., & Pakull, M. 2004, MNRAS, 349, 39
Cuillandre, J., Lequeux, J., Allen, R. J., Mellier, Y., & Bertin, E. 2001, ApJ, 554, 190

Dale, D. A., & Helou, G. 2002, ApJ, 576, 159
Davies, J. I., & Burstein, D. 1995, The Opacity of Spiral Disks (Dordrecht: Kluwer)
de Jong, R. S. 1996, A&A, 313, 377
de Vaucouleurs, G., de Vaucouleurs, A., Corwin, H. G., Jr., Buta, R. J., Paturel, G., & Fouqué, P. 1991, Third Reference Catalogue of Bright Galaxies (New York: Springer) (RC3)
Disney, M., Davies, J., & Phillipps, S. 1989, MNRAS, 239, 939
Domingue, D. L., Keel, W. C., Ryder, S. D., & White, R. E. 1999, AJ, 118, 1542
Domingue, D. L., Keel, W. C., & White, R. E. 2000, ApJ, 545, 171
Ferrarese, L., et al. 1996, ApJ, 464, 568
———. 1998, ApJ, 507, 655
Freedman, W. L., et al. 1994, ApJ, 427, 628
———. 2001, ApJ, 553, 47
Gehrels, N. 1986, ApJ, 303, 336
Gibson, B. K., et al. 1999, ApJ, 512, 48
Giovanelli, R., Haynes, M. P., Salzer, J. J., da Costa, L. N., & Freudling, W. 1994, AJ, 107, 2036
———. 1995, AJ, 110, 1059
González, R. A., Allen, R. J., Dirsch, B., Ferguson, H. C., Calzetti, D., & Panagia, N. 1998, ApJ, 506, 152
González, R. A., Fruchter, A. S., & Dirsch, B. 1999, ApJ, 515, 69
González, R. A., Loinard, L., Allen, R. J., & Muller, S. 2003, AJ, 125, 1182
Graham, A. W. 2001, MNRAS, 326, 543
Graham, J. A., et al. 1997, ApJ, 477, 535
———. 1999, ApJ, 516, 626
Helou, G., Lu, N. Y., Werner, M. W., Malhotra, S., & Silbermann, N. 2000, ApJ, 532, L21
Holmberg, E. 1958, Medde. Lunds Astron. Obs., Ser. II, 136, 1
Holwerda, B. W. 2005, Ph.D. thesis, Univ. Groningen
Holwerda, B. W., Allen, R. J., & van der Kruit, P. C. 2002, in ASP Conf. Ser. 273, The Dynamics, Structure & History of Galaxies, ed. G. S. da Costa & H. Jerjen (San Francisco: ASP), 337
Holwerda, B. W., González, R. A., Allen, R. J., & van der Kruit, P. C. 2005, AJ, 129, 1381
Hughes, S. M. G., et al. 1998, ApJ, 501, 32
Jablonka, P., Bica, E., Bonatto, C., Bridges, T. J., Langlois, M., & Carter, D. 1998, A&A, 335, 867
Keel, W. C., & White, R. E. 2001a, AJ, 121, 1442
———. 2001b, AJ, 122, 1369
Kelson, D. D., et al. 1999, ApJ, 514, 614
Kim, J. H., & McGaugh, S. S. 2002, BAAS, 34, 1115
Larsen, S. S. 2004, A&A, 416, 537
Leonard, D. C., Kanbur, S. M., Ngeow, C. C., & Tanvir, N. R. 2002a, BAAS, 34, 1143
Leonard, D. C., et al. 2002b, PASP, 114, 35
Liu, J., Bregman, J. N., & Seitzer, P. 2002, ApJ, 580, L31
Macri, L. M., Stetson, P. B., Bothun, G. D., Freedman, W. L., Garnavich, P. M., Jha, S., Madore, B. F., & Richmond, M. W. 2001, ApJ, 559, 243
Macri, L. M., et al. 1999, ApJ, 521, 155
Masters, K. L., Giovanelli, R., & Haynes, M. P. 2003, AJ, 126, 158
Mayya, Y. D., & Rengarajan, T. N. 1997, AJ, 114, 946
Mould, J. R., et al. 2000, ApJ, 528, 655
Newman, J. A., Zepf, S. E., Davis, M., Freedman, W. L., Madore, B. F., Stetson, P. B., Silbermann, N., & Phelps, R. 1999, ApJ, 523, 506
O'Neil, K., Bothun, G. D., & Impey, C. D. 2000, ApJS, 128, 99
Ostriker, J. P., & Heisler, J. 1984, ApJ, 278, 1
Peletier, R. F., & Willner, S. P. 1992, AJ, 103, 1761
Pierce, M. J., Welch, D. L., McClure, R. D., van den Bergh, S., Racine, R., & Stetson, P. B. 1994, Nature, 371, 385
Rawson, D. M., et al. 1997, ApJ, 490, 517
Roennback, J., & Shaver, P. A. 1997, A&A, 322, 38
Saha, A., Sandage, A., Labhardt, L., Tammann, G. A., Macchetto, F. D., & Panagia, N. 1996a, ApJ, 466, 55
———. 1996b, ApJS, 107, 693
Saha, A., Sandage, A., Tammann, G. A., Labhardt, L., Macchetto, F. D., & Panagia, N. 1999, ApJ, 522, 802
Saha, A., Sandage, A., Thim, F., Labhardt, L., Tammann, G. A., Christensen, J., Panagia, N., & Macchetto, F. D. 2001, ApJ, 551, 973
Sakai, S., Ferrarese, L., Kennicutt, R. C., & Saha, A. 2004, ApJ, 608, 42
Sakai, S., et al. 1999, ApJ, 523, 540
Sandage, A., Saha, A., Tammann, G. A., Labhardt, L., Panagia, N., & Macchetto, F. D. 1996, ApJ, 460, L15
Schlegel, D. J., Finkbeiner, D. P., & Davis, M. 1998, ApJ, 500, 525
Silbermann, N. A., et al. 1996, ApJ, 470, 1
———. 1999, ApJ, 515, 1
Tully, R. B., Pierce, M. J., Huang, J., Saunders, W., Verheijen, M. A. W., & Witchalls, P. L. 1998, AJ, 115, 2264
Turner, A., et al. 1998, ApJ, 505, 207
Valentijn, E. A. 1990, Nature, 346, 153
———. 1994, MNRAS, 266, 614
White, R. E., & Keel, W. C. 1992, Nature, 359, 129
White, R. E., Keel, W. C., & Conselice, C. J. 2000, ApJ, 542, 761